

RESEARCH PAPER

# Combination of *in vivo* proximity labeling and co-immunoprecipitation identifies the host target network of a tumor-inducing effector in the fungal maize pathogen *Ustilago maydis*

Wei Shi<sup>1,2</sup>, Sara C. Stolze<sup>3</sup>, Hirofumi Nakagami<sup>3,4</sup> , Johana C. Misas Villamil<sup>1,2</sup> , Isabel M.L. Saur<sup>1,2</sup> and Gunther Doehlemann<sup>1,2,\*</sup> 

<sup>1</sup> Institute for Plant Sciences University of Cologne, D-50674 Cologne, Germany

<sup>2</sup> Cluster of Excellence on Plant Sciences (CEPLAS), Germany

<sup>3</sup> Protein Mass Spectrometry, Max-Planck Institute for Plant Breeding Research, Carl-von-Linné-Weg 10, D-50829 Cologne, Germany

<sup>4</sup> Basic Immune System of Plants, Max-Planck Institute for Plant Breeding Research, Carl-von-Linné-Weg 10, D-50829 Cologne, Germany

\* Correspondence: [g.doehlemann@uni-koeln.de](mailto:g.doehlemann@uni-koeln.de)

Received 5 January 2023; Editorial decision 5 May 2023; Accepted 18 May 2023

Editor: Bjorn Usadel, Forschungszentrum Jülich, Germany

## Abstract

Plant pathogens secrete effectors, which target host proteins to facilitate infection. The *Ustilago maydis* effector UmSee1 is required for tumor formation in the leaf during infection of maize. UmSee1 interacts with maize SGT1 (suppressor of G2 allele of *skp1*) and blocks its phosphorylation *in vivo*. In the absence of UmSee1, *U. maydis* cannot trigger tumor formation in the bundle sheath. However, it remains unclear which host processes are manipulated by UmSee1 and the UmSee1–SGT1 interaction to cause the observed phenotype. Proximity-dependent protein labeling involving the turbo biotin ligase tag (TurboID) for proximal labeling of proteins is a powerful tool for identifying the protein interactome. We have generated transgenic *U. maydis* that secretes biotin ligase-fused See1 effector (UmSee1–TurboID-3HA) directly into maize cells. This approach, in combination with conventional co-immunoprecipitation, allowed the identification of additional UmSee1 interactors in maize cells. Collectively, our data identified three ubiquitin–proteasome pathway-related proteins (ZmSIP1, ZmSIP2, and ZmSIP3) that either interact with or are close to UmSee1 during host infection of maize with *U. maydis*. ZmSIP3 represents a cell cycle regulator whose degradation appears to be promoted in the presence of UmSee1. Our data provide a possible explanation of the requirement for UmSee1 in tumor formation during *U. maydis*–*Zea mays* interaction.

**Keywords:** Fungal effectors, maize, protein interactome, TurboID, ubiquitin–proteasome, *Ustilago maydis*.

## Introduction

Most staple crops are essential for food security. Plant diseases greatly threaten food security by limiting the yield and quality of crops (Fisher *et al.*, 2016). Pathogens secrete effectors to target host structures for spreading infection (Dodds and Rathjen, 2010). Effectors usually modulate the biological activity of host proteins to suppress plant immunity (Hogenhout *et al.*, 2009). Identifying effector targets in the plant aids in the understanding of pathogenic mechanisms and thereby improves resistance to crop pathogens. The location, specificity, and low effector protein levels *in planta* are major obstacles for the identification of host target proteins.

*Ustilago maydis* is a plant fungal pathogen causing corn smut of many important crops and grasses, including the widely grown food and energy crop maize (*Zea mays*) (Kahmann and Kämper, 2004; Doehlemann *et al.*, 2008). *Ustilago maydis* induces tumors on all aerial parts of maize and suppresses plant immunity by secreting effectors to the plant tissue (Skibbe *et al.*, 2010). Plant tumors produced upon *U. maydis* infection have been defined as clusters of cells that present abnormal cell division and reduced cell differentiation. The cell cycle is responsible for DNA replication and cell division, and it is well known that an abnormal cell cycle causes tumors in animals and plants (Jacobs *et al.*, 1999). *Ustilago maydis* induces such tumors on all aerial parts of maize, which is a complex and dynamic process. The *U. maydis*-induced leaf tumor formation at the cellular level is composed of hypertrophic and hyperplastic tumor cells resulting from transformed mesophyll cells and bundle sheath cells, respectively (Matei *et al.*, 2018). About 460 effectors encoded by *U. maydis* target different host compartments (Lanver *et al.*, 2017). Only a few have been functionally characterized, including Pep1, Pit2, Cmu1, Tin2, See1, Mer1, Rip1, and Tips (Doehlemann *et al.*, 2009; Djamei *et al.*, 2011; Mueller *et al.*, 2013; Tanaka *et al.*, 2014; Redkar *et al.*, 2015a; Misas Villamil *et al.*, 2019; Darino *et al.*, 2021; Navarrete *et al.*, 2021; Bindics *et al.*, 2022; Saado *et al.*, 2022).

Interestingly, the organ-specific UmSee1 effector is required for the trans-differentiation of bundle sheath cells into hypertrophic tumor cells but not for the hypertrophic cells' enlargement in the mesophyll cells, and the UmSee1-induced tumor formation and expansion only occur in vegetative tissues but not in floral tissues (Redkar *et al.*, 2015a). The UmSee1 effector is translocated from biotrophic hyphae to the plant cytoplasm and nucleus, and a yeast two-hybrid (Y2H) screen demonstrated the interaction of UmSee1 with maize SGT1 (suppressor of G2 allele of *skp1*) (Redkar *et al.*, 2015a). Several regulators control cell cycle progression, including cyclin-dependent kinases (CDKs), cell division control proteins (CDCs), cyclin proteins (CYCs), anaphase-promoting complex (APCs), and other activators or suppressors (Dang *et al.*, 2021). The previously identified UmSee1-interactor SGT1 is required for both the G<sub>1</sub>/S and G<sub>2</sub>/M cell cycle transitions in yeast, and it is highly conserved in eukaryotic cells (Kitagawa

*et al.*, 1999). Although UmSee1-mediated inhibition of mitogen-activated protein kinase (MAPK)-triggered SGT1 phosphorylation could be detected (Redkar *et al.*, 2015a), it remains elusive how SGT1 affects the plant cell cycle and how the cell cycle is influenced by UmSee1.

To provide further insight into this key question and to minimize the individual limitations of each protein–protein interaction assay, we complemented the previously performed Y2H screen (Redkar *et al.*, 2015a) with state-of-the-art *de novo* identification of UmSee1 interactors *in planta*. We applied co-immunoprecipitation (Co-IP) and established proximity labeling (PL) for TurboID-catalyzed biotinylation of intracellular maize proteins upon *U. maydis*-mediated delivery of TurboID-fused UmSee1. Co-IP is very effective in obtaining stable complexes, but weak or transient interactors are not detected (Ngounou Wetie *et al.*, 2014; Sciuto *et al.*, 2019). PL captures weak or transient protein interactions and also proteins that locate consistently in close proximity to the protein of interest (Gingras *et al.*, 2019). Biotin-based PL approaches have been applied in yeast, plants, and animals, including *Schizosaccharomyces pombe*, *Caenorhabditis elegans*, *Arabidopsis thaliana*, and *Nicotiana benthamiana*, using transient expression or transgenic lines for specific cellular proteomes as well as interaction networks of nuclear, cytosolic, and membrane baits (Branon *et al.*, 2018; Conlan *et al.*, 2018; Larochelle *et al.*, 2019; Mair *et al.*, 2019; Zhang *et al.*, 2019; Holzer *et al.*, 2022; Melkonian *et al.*, 2022). In the present study, we used a transgenic *U. maydis* strain to directly deliver UmSee1–TurboID–3HA fusion protein into maize cells during the infection process. This approach produced distinct datasets of putative UmSee1-interacting candidates collectively suggesting a function of UmSee1 within the ubiquitin–proteasome network, a pathway also involving SGT1 (Dielen *et al.*, 2010). We confirmed three *Zea mays* UmSee1 interacting proteins (ZmSIPs) in further analyses and found them to also associate with the previously identified See1 target ZmSGT1. All three ZmSIPs are implicated in the ubiquitin–proteasome pathway. Moreover, the presence of UmSee1 is linked to a more rapid degradation of ZmSIP3, a cell cycle regulator 48 (CDC48), by the maize proteasome.

## Materials and methods

### Plasmid construction

NEBuilder HiFi DNA assembly (Gibson cloning method) was used for all cloning processes. For the transformation of *U. maydis*, the plasmid p123-P<sub>Pit2</sub>-TurboID-3HA containing the native promoter of UmPit2 (UMAG\_01375), TurboID, and a 3HA tag was generated using NEBuilder HiFi DNA Assembly. This plasmid was then used to generate the p123-P<sub>Pit2</sub>-SP<sub>UmSee1</sub>-mCherry-TurboID-3HA and the p123-P<sub>Pit2</sub>-UmSee1-TurboID-3HA also using NEBuilder HiFi DNA Assembly. All constructs were confirmed by sequencing. For Y2H assays, cDNAs of mCherry and ZmSIPs (ZmSIP1, ZmSIP2, and ZmSIP3) were cloned into the pGADT7 vector (Clontech) for expression via the

GAL4 activation domain (AD) under the constitutive ADH1 promoter. mCherry, UmSee1 $\Delta$ SP, SrSee1 $\Delta$ SP, and UhSee1 $\Delta$ SP were cloned into the pGBKT7 vector (Clontech) for expression with the GAL4 DNA-binding domain (BD) under control of the constitutive ADH1 promoter. For Co-IP and *in vivo* protein degradation assays, cDNAs of green fluorescent protein (GFP) and ZmSIP1, ZmSIP2, and ZmSIP3 lacking stop codons were cloned into the pICH47732 vector with the cauliflower mosaic virus (CaMV) 35S promoter and a 4myc tag, and coding sequences (CDSs) of UmSee1 $\Delta$ SP and ZmSGT1 were cloned into the pICH47732 vector with the CaMV 35S promoter and a 6HA tag. For subcellular localization studies, ZmSIP1, ZmSIP2, and ZmSIP3 lacking stop codons were cloned into the pICH47732 vector with the 35S promoter and a GFP tag. UmSee1 $\Delta$ SP was cloned into the pICH47732 vector with the 35S promoter and an mCherry tag. For UmSee1 $\Delta$ SP protein expression in *Escherichia coli* and subsequent activity-based protein profiling (ABPP), the UmSee1 CDS was amplified by PCR without its signal peptide (SP) and ligated into the pET15b vector. All primers used are listed in [Supplementary Table S1](#).

#### Generation of fungal strains and growth conditions

The *U. maydis* strains generated and used in this study are listed in [Supplementary Table S2](#). The p123-P<sub>Pit2</sub>-UmSee1-TurboID-3HA and p123-P<sub>Pit2</sub>-SP<sub>UmSee1</sub>-mCherry-TurboID-3HA constructs containing the carboxin resistance *ip* allele were introduced into *U. maydis* strains SG200 $\Delta$ See1 and SG200, respectively, via homologous recombination in the *ip* locus (Kämper, 2004). All generated *U. maydis* strains were confirmed by PCR and Southern blot. The *U. maydis* strains were grown in liquid YEPS light medium on a shaker (200 rpm) or potato dextrose agar (PD) plates at 28 °C.

#### Plant infections

For assessing virulence, 7-day-old maize seedlings of Early Golden Bantam (EGB) were inoculated with *U. maydis* strains with an OD<sub>600</sub>=1.0. Disease symptoms were scored at 12 days post-infection (dpi) as described (Kämper *et al.*, 2006) and the experiment was performed at least three times independently.

#### Sample preparation for TurboID and mass spectrometry

For the preparation of samples for TurboID, 7-day-old maize seedlings of EGB were inoculated with the respective *U. maydis* strains (pPit2:SP<sub>UmSee1</sub>-mCherry-TurboID-3HA and pPit2:UmSee1-TurboID-3HA) at an OD<sub>600</sub>=3.0. A high concentration of biotin dissolved in water with a final concentration of 100  $\mu$ M was used as the infiltration solution. The biotin infiltration solution was directly injected into the infection site of maize leaves using a syringe at 2 dpi. For each construct, three biological replicates were performed and analyzed via MS. For each biological replicate, at least 20 biotin-treated maize leaves were harvested at 3 dpi (2 d post-biotin treatment) and frozen in liquid nitrogen. Frozen plant material was ground to a fine powder for protein extraction. These plant powders were separated and placed into 2 ml Eppendorf tubes.

For TurboID-based PL, one tube containing frozen powder was added to 500  $\mu$ l of SDT-lysis buffer (10 ml of 10% SDS, 2.5 ml of 1 M DTT, 2.5 ml of 1 M Tris pH 7.5, 10 ml of ddH<sub>2</sub>O) (Melkonian *et al.*, 2022), and incubated for 5 min at 95 °C after vortex mixing. The samples were sonicated for 10 min and centrifuged for 10 min at 13 300 g. The resulting supernatant was transferred to a fresh tube as total proteins. Biotin depletion of the total proteins used the methanol-chloroform precipitation method (Melkonian *et al.*, 2022). A 666  $\mu$ l aliquot of methanol and 166  $\mu$ l of chloroform were added to 500  $\mu$ l of total protein extracts and mixed with 300  $\mu$ l of ddH<sub>2</sub>O. The mix was centrifuged for 10 min at 1500 g and the supernatant was discarded; the protein pellets were washed

by 600  $\mu$ l methanol twice and air-dried for 5 min, then resuspended in 500  $\mu$ l of SDT-lysis buffer and incubated on an Eppendorf Thermomixer for 30 min at 1250 rpm with shaking. The biotin-depleted samples were diluted with phosphate-buffered saline (PBS; 0.1 M phosphate, 0.15 M NaCl, pH 7.2) to a final concentration of 0.5% SDS. Streptavidin-agarose beads (Thermo Fisher Scientific) were washed with PBS three times. After adding 50  $\mu$ l of beads to each sample, the samples were incubated on a rolling wheel at room temperature for 20 h. The beads were centrifuged for 3 min at 3500 rpm and the supernatant was removed, then washed once with 2 ml of PBS containing 2% SDS and six times with 10 ml of PBS. An aliquot of the beads was used for immunoblotting; the antibody used was horseradish peroxidase (HRP)-conjugated streptavidin (Strep-HRP, 1:1000 dilution; Sigma-Aldrich). For HA-IP, one tube containing frozen powder was added to 1.5 ml of ice-cold protein-lysis buffer [50 mM Tris pH 7.5, 150 mM NaCl, 1 0% glycerol, 2 mM EDTA, 10 mM DTT, 0.5% IGEPAL, 1 mM phenylmethylsulfonyl fluoride (PMSF)] with cComplete™ Protease Inhibitor Cocktail (Roche) and incubated on ice for half an hour after vortexing. The tubes were centrifuged at 13 300 g for 10 min at 4 °C, the upper soluble fraction was centrifuged again at 13 300 g for 20 min at 4 °C, and the resulting supernatant was transferred to a fresh tube as total protein extract. HA magnetic beads (Pierce Anti-HA magnetic beads, Thermo Fisher Scientific) were separated on a magnetic separator and washed three times by ice-cold wash buffer (50 mM Tris-HCl pH 7.5, 150 mM NaCl, 10% glycerol, 2 mM EDTA). After adding 10  $\mu$ l of beads to each of the cell extracts, the samples were incubated on a rolling wheel at 4 °C for 3 h. HA magnetic beads were magnetically separated and washed in 1 ml of wash buffer three times. An aliquot of the beads was used for immunoblotting; the antibodies used were mouse anti-HA primary antibody (1:30 000 dilution; Sigma-Aldrich) and anti-mouse IgG secondary antibody (1:10 000 dilution; Thermo Fisher Scientific).

#### Identification of proteins by LC-MS

Proteins from HA enrichment were submitted to an on-bead digestion. In brief, dry beads were re-dissolved in 25  $\mu$ l of digestion buffer 1 (50 mM Tris, pH 7.5, 2 M urea, 1 mM DTT, 5 ng  $\mu$ l<sup>-1</sup> trypsin) and incubated for 30 min at 30 °C in a Thermomixer at 400 rpm. Next, beads were pelleted and the supernatant was transferred to a fresh tube. A 50  $\mu$ l aliquot of digestion buffer 2 (50 mM Tris, pH 7.5, 2 M urea, 5 mM chloroacetamide) was added to the beads. After mixing, the beads were pelleted and the supernatant was collected and combined with the previous one. The combined supernatants were then incubated overnight at 32 °C in a Thermomixer with 400 rpm; samples were protected from light during incubation. The digestion was stopped by adding 1  $\mu$ l of trifluoroacetic acid (TFA) and desalted with C18 Empore disk membranes according to the StageTip protocol (Rappsilber *et al.*, 2003). For streptavidin pull-down, double the amounts of buffers were used (Melkonian *et al.*, 2022). Dried peptides were re-dissolved in 2% acetonitrile (ACN), 0.1% TFA (10  $\mu$ l) and diluted to 0.1  $\mu$ g  $\mu$ l<sup>-1</sup> for analysis. Samples were analyzed using an EASY-nLC 1200 (Thermo Fisher Scientific) coupled to a Q Exactive Plus mass spectrometer (Thermo Fisher Scientific). Peptides were separated on 16 cm frit-less silica emitters (New Objective, 75  $\mu$ m inner diameter), packed in-house with reversed-phase ReproSil-Pur C18 AQ 1.9  $\mu$ m resin. Peptides were loaded on the column and eluted for 115 min using a segmented linear gradient of 5–95% solvent B (0 min: 5% B; 0–5 min  $\rightarrow$ 5% B; 5–65 min  $\rightarrow$ 20% B; 65–90 min  $\rightarrow$ 35% B; 90–100 min  $\rightarrow$ 55%; 100–105 min  $\rightarrow$ 95%, 105–115 min  $\rightarrow$ 95%) [solvent A 0% ACN, 0.1% formic acid (FA); solvent B 80% ACN, 0.1% FA] at a flow rate of 300 nl min<sup>-1</sup>. Mass spectra were acquired in data-dependent acquisition mode with a TOP15 method. MS spectra were acquired in the Orbitrap analyzer with a mass range of 300–1750 *m/z* at a resolution of 70 000 FWHM (full width at half maximum) and a target value of 3  $\times$  10<sup>6</sup> ions. Precursors were selected with an isolation window of

1.3 *m/z*. HCD (higher energy collisional dissociation) fragmentation was performed at a normalized collision energy of 25. MS/MS spectra were acquired with a target value of  $10^5$  ions at a resolution of 17 500 FWHM, a maximum injection time of 55 ms, and a fixed first mass of *m/z* 100. Peptides with a charge of +1, >6, or with unassigned charge state were excluded from fragmentation for MS<sup>2</sup>; dynamic exclusion for 30 s prevented repeated selection of precursors.

The MS proteomics data have been deposited to the ProteomeXchange Consortium via the PRIDE partner repository with the dataset identifier PXD040939 (Perez-Riverol *et al.*, 2022). Raw data were processed using MaxQuant software (version 1.6.3.4, <http://www.maxquant.org/>) with label-free quantification (LFQ) and iBAQ (intensity-based absolute quantification) enabled (Cox and Mann, 2008; Tyanova *et al.*, 2016). MS/MS spectra were searched by the Andromeda search engine against a combined database containing the sequences from *Z. mays* (Zm-B73-REFERENCE-NAM-5.0) from EnsemblPlants (<https://plants.ensembl.org/>) and sequences of 248 common contaminant proteins and decoy sequences. Trypsin specificity was required and a maximum of two missed cleavages allowed. Minimal peptide length was set to seven amino acids. Carbamidomethylation of cysteine residues was set as fixed, and oxidation of methionine and protein N-terminal acetylation as variable modifications. Peptide spectrum matches and proteins were retained if they were below a false discovery rate (FDR) of 1%.

Statistical analysis of the MaxLFQ values was carried out using Perseus (version 1.5.8.5, <http://www.maxquant.org/>). Quantified proteins were filtered for reverse hits, and hits ‘identified by site’ and MaxLFQ values were log<sub>2</sub> transformed. After grouping samples by condition, only those proteins were retained for the subsequent analysis that had two valid values in one of the conditions. Two-sample *t*-tests were performed using a permutation-based FDR of 5%. Alternatively, quantified proteins were grouped by condition, and only those hits were retained that had three valid values in one of the conditions. Missing values were imputed from a normal distribution (1.8 downshift, separately for each column). Volcano plots were generated in Perseus using an FDR of 5% and an S0=1. The Perseus output was exported and further processed using Excel. Relative iBAQ values were calculated per column from MaxQuant output, scaled by a factor of  $10^6$  and log<sub>10</sub> transformed (Melkonian *et al.*, 2022).

#### Protein–protein interactions (PPIs) and Gene Ontology (GO) enrichment analysis

PPI analysis was done by using the STRING database (<https://string-db.org/>) (Szklarczyk *et al.*, 2021), then further analyzed by Cytoscape software (version 3.9.1, <https://cytoscape.org/>) with CluePedia (version 1.5.9, <https://apps.cytoscape.org/apps/cluepedia>) and ClueGo (version 2.5.9, <https://apps.cytoscape.org/apps/cluego>) (Shannon *et al.*, 2003; Bindea *et al.*, 2009, 2013; Mlecnik *et al.*, 2019). The GO and Kyoto Encyclopedia of Genes and Genomes (KEGG) enrichment analysis was done by ShinyGO v0.66 (<http://bioinformatics.sdstate.edu/go65/>) (Ge *et al.*, 2020).

#### Yeast-two hybrid assay

The pGBKT7 and pGADT7 plasmids were co-transformed into yeast strain AH109 (Clontech) using the LiCl–PEG (polyethylene glycol) method (Paiano *et al.*, 2019). Yeast transformants were selected on SD–Leu–Trp plates and grown in liquid SD–Leu–Trp for 16 h before washing in ddH<sub>2</sub>O. The cell density was adjusted to OD<sub>600</sub>=1.0 and a dilution series was dropped out on SD–Leu–Trp and SD–Leu–Trp–His plates. Plates were incubated for 5 d at 28 °C. At least five independent clones were tested for each combination.

#### *Agrobacterium*-mediated transformation of *Nicotiana benthamiana* leaves

Plasmids of interest were transformed into *Agrobacterium tumefaciens* GV3101 pmp90. Single transformants were confirmed by colony PCR and grown in a liquid dYT medium containing the corresponding antibiotics at 28 °C for 16 h. Bacterial cells were harvested and resuspended in infiltration buffer (10 mM MES, pH 5.6, 10 mM MgCl<sub>2</sub>, 200 μM acetosyringone) to a final OD<sub>600</sub>=1.0. The different cultures were mixed equally and then infiltrated into the leaves of 4-week-old *N. benthamiana* plants.

#### Co-immunoprecipitation and immunoblotting

Leaves transformed with the constructs of interest were harvested at 3 dpi and frozen in liquid nitrogen. Frozen plant material was ground to a fine powder with 1.5 ml of ice-cold protein lysis buffer (50 mM Tris pH 7.5, 150 mM NaCl, 10 % glycerol, 2 mM EDTA, 10 mM DTT, 0.5 % IGEPAL, 1 mM PMSF) containing cOmplete™ Protease Inhibitor Cocktail (Roche) for protein extraction. The protein extracts were centrifuged twice, and the resulting supernatant was transferred to a fresh tube as input; an aliquot of the input was used for immunoblotting. A 5 μl aliquot of washed Myc magnetic beads (Chromotek) was added to the protein extracts of each sample, and samples were then incubated on a rolling wheel at 4 °C. Myc magnetic beads were magnetically separated and washed in 1 ml of wash buffer three times. The elution proteins were eluted from the beads with 2× SDS loading buffer (125 mM Tris–HCl pH 6.8, 20% glycerol, 4% SDS, 0.04% bromophenol blue) for immunoblotting.

The input or eluted proteins were separated by SDS–PAGE gels using gel electrophoresis (Bio–Rad), and blotted onto polyvinylidene fluoride (PVDF) membranes (Merck) using a Trans-Blot Turbo (Bio–Rad) transfer system. The membranes were blocked in TBST with 3% non-fat milk. The antibodies used were mouse anti-HA primary antibody (1:30 000 dilution; Sigma–Aldrich), anti-mouse IgG secondary antibody (1:10 000 dilution; Thermo Fisher Scientific), rabbit anti-myc primary antibody (1:5000 dilution; Abcam), and anti-rabbit IgG secondary antibody (1:3000 dilution; Cell Signaling). The membranes were probed with primary antibody for 2 h or overnight and secondary antibody for 1 h. TBST-washed membranes were detected with the SuperSignal luminol-based chemiluminescent substrate (Thermo Fisher Scientific) by the CCD imaging system (ChemiDoc, Bio–Rad).

#### Split-luciferase complementation (split-LUC) assay

Split-LUC assays in *N. benthamiana* were performed as described (Zhou *et al.*, 2018). *Agrobacterium*-mediated transformation of *N. benthamiana* leaves was performed as described above. For luciferase measurements, leaves were harvested 2 dpi and sprayed with 1 mM D–luciferin for 10 min in the dark. The luminescence signals of the leaves from three independent plants were detected by the CCD imaging system (ChemiDoc, Bio–Rad).

#### Purification of Umsee1 and activity-based protein profiling

The pET15b–UmSee1ΔSP plasmid was transformed into Rosetta (DE3) competent cells, and recombinant protein expression was initiated by 0.1 mM isopropyl-β-D-thiogalactopyranoside (IPTG) treatment at OD<sub>600</sub>=0.6–0.8. Then cells were incubated at 18 °C with shaking at 120 rpm for 18 h. Cells were harvested and lysed using a microfluidizer. 6His–UmSee1ΔSP protein was purified using affinity chromatography with an Ni–NTA column (Thermo Fisher Scientific) and further purified using size exclusion chromatography with a HiLoad Superdex 75 16/600 column (GE–Healthcare) (Li and Sousa, 2012). The ABPP assays

were performed as described before (Kolodziejek *et al.*, 2011; Misas-Villamil *et al.*, 2017). In brief, maize leaves were ground and resuspended in 50 mM Tris-HCl buffer (pH 7). The supernatant was pre-incubated for 30 min with 5  $\mu$ M (final concentration) BSA or recombinant 6His-UmSee1 $\Delta$ SP or with 20  $\mu$ M (final concentration) epoxomicin or DMSO. Then, samples were incubated with 1  $\mu$ M (final concentration) of the proteasome probe MVB072 for 2 h. Samples were denatured at 95 °C in 2 $\times$  SDS loading buffer and separated on SDS-PAGE gels. The probe was detected using the rhodamine filter (excitation, 532 nm; emission, 580 nm) on a ChemiDoc (Bio-Rad). The gel was stained with SyproRuby (Invitrogen) to determine equal loading according to the manufacturer's instructions. Quantification of the signals was performed by Image J (Schneider *et al.*, 2012); all the images were transformed into gray-scale and 8-bit type for further analysis. The intensity was normalized to the loading control first, then the final signals were normalized to the epoxomicin control.

#### Protein degradation assay

Protein degradation assays were performed as described before (Liu *et al.*, 2010). In brief, *N. benthamiana* leaves expressing mCherry-6HA, UmSee1 $\Delta$ SP-mCherry-6HA, and ZmSIPs-4myc proteins were harvested 3 dpi and frozen in liquid nitrogen. Frozen plant material was ground to a fine powder with 1.0 ml of ice-cold lysis buffer (250 mM Tris pH 7.5, 150 mM NaCl, 10 % glycerol) for protein extraction. The protein extracts were centrifuged twice at 13 000 g for 20 min, and the resulting supernatant was transferred to a fresh tube. ZmSIPs-4myc protein extracts were mixed in different proportions with mCherry-6HA or UmSee1 $\Delta$ SP-mCherry-6HA protein extracts and treated with 100  $\mu$ M (final concentration) proteasome inhibitor MG132 or DMSO for 45 min at 28 °C. The reactions were stopped by boiling samples at 95 °C in 2 $\times$  SDS loading buffer for 10 min, and separated on SDS-PAGE gels. Samples were analyzed by western blot using anti-myc and anti-HA at concentrations specified above. The membrane was stained with Coomassie brilliant blue to determine equal protein loading.

#### Subcellular localization assay

At 3 d post-transformation of *N. benthamiana* leaves, fluorescent signals were analyzed using a Leica TCS SP8 confocal laser scanning microscope (Leica) employing filters for GFP (excitation 458 nm and emission 470–490 nm) and mCherry (excitation 561 nm and emission 590–603 nm).

## Results

### Establishment of TurboID-based proximity labeling in the *U. maydis*-maize pathosystem

A previous study demonstrated that UmSee1 is secreted into host cells during *U. maydis* infection of maize leaves and that it can interact with the *Z. mays* SGT1 homolog (Redkar *et al.*, 2015a). To explore the potential for identifying further UmSee1-interacting proteins and proteins in close proximity to UmSee1 in maize leaves, we aimed to directly transfer TurboID-fused UmSee1 proteins (UmSee1-TurboID-3HA) from biotrophic fungal hyphae into host cells (Fig. 1A). TurboID activates biotin molecules to bind to exposed lysines of neighboring proteins, which allows non-toxic biotin labeling in 10 min with much less biotin (Branon *et al.*, 2018). The biotinylated proteins' binding affinity for streptavidin beads does not rely on the native state or the ligase activity, which is advantageous

for denatured protein extraction and binding in the presence of a high amount of detergents for subcellular compartments, including membrane proteins (Stayton *et al.*, 1999). We generated UmSee1 fused C-terminally to a TurboID-3HA tag and expressed it under control of the *pit2* promoter, which confers a high expression level *in planta* (Doehlemann *et al.*, 2011). The construct (*pPit2:UmSee1-TurboID-3HA*, Fig. 1B) was expressed in the *see1* knockout strain SG200 $\Delta$ see1 which allowed us to confirm that the recombinant effector protein fully complemented the virulence defect of the SG200 $\Delta$ see1 strain (Fig. 1C; Supplementary Table S3). Anti-HA western blot analysis confirmed the successful enrichment of the fusion proteins (Fig. 1D). To select specificity in the following experiments, the mCherry protein was fused to the SP of UmSee1 (*pPit2:SP<sub>UmSee1</sub>-mCherry-TurboID-3HA*, Fig. 1B) and expressed in *U. maydis* SG200, also under the *pit2* promoter. Maize leaves infected with the two *U. maydis* strains and infiltrated with 100  $\mu$ M biotin for biotin-mediated labeling were subjected to protein extraction at 3 dpi under native (anti-HA) and denaturing (TurboID) conditions. Plant protein extracts were subjected to anti-HA immunoprecipitation and isolation of biotinylated proteins, followed by LC-MS/MS for the identification of isolated proteins (Fig. 1E). Biotinylation of maize proteins by secreted UmSee1-TurboID-3HA was confirmed by Strep-HRP western blot of raw protein extracts and streptavidin-enriched samples after treatment of the samples with 100  $\mu$ M biotin (Supplementary Fig. S1A). We detected enhanced biotinylation of maize proteins in the samples carrying UmSee1 compared with the mCherry control samples (Supplementary Fig. S1B). Three biological replicates of HA-IP and TurboID were sampled from the identical plant for subsequent LC-MS/MS analysis.

The relative amount of each identified protein within each replicate group was quantified by LC-MS/MS using LFQ, and protein abundances with a sample were quantified using iBAQ (Tyanova *et al.*, 2016). The data were analyzed by a *t*-test-based analysis ( $\geq 2$  valid LFQ values) and volcano plot analysis (three valid LFQ values). We identified 2563 and 1342 proteins in HA-IP and TurboID-based PL from the volcano plot analysis results, respectively (Supplementary Table S4). High Pearson correlation values ( $r > 0.95$ ) among the biological replicates of HA-IP and TurboID-based PL datasets indicate reproducibility of the data. To determine the interactors or enrichment, we used the raw data to calculate two-sample *t*-tests with a permutation-based FDR of 5%. The enriched interactors of UmSee1 were designated if they had a *P*-value  $< 0.05$  and log<sub>2</sub> fold change  $> 1$  over the control (Fig. 2A). Finally, 262 and 67 proteins were identified by HA-IP and TurboID-based PL, respectively, and, of these, 11 proteins were identified by both approaches (Supplementary Fig. S1C; Supplementary Table S5). The datasets were further analyzed separately or together by PPI analysis using the STRING database, and GO or KEGG enrichment analysis using ShinyGO v0.66 (Fig. 2B–D; Supplementary Figs S2, S3). PPI and GO results suggest

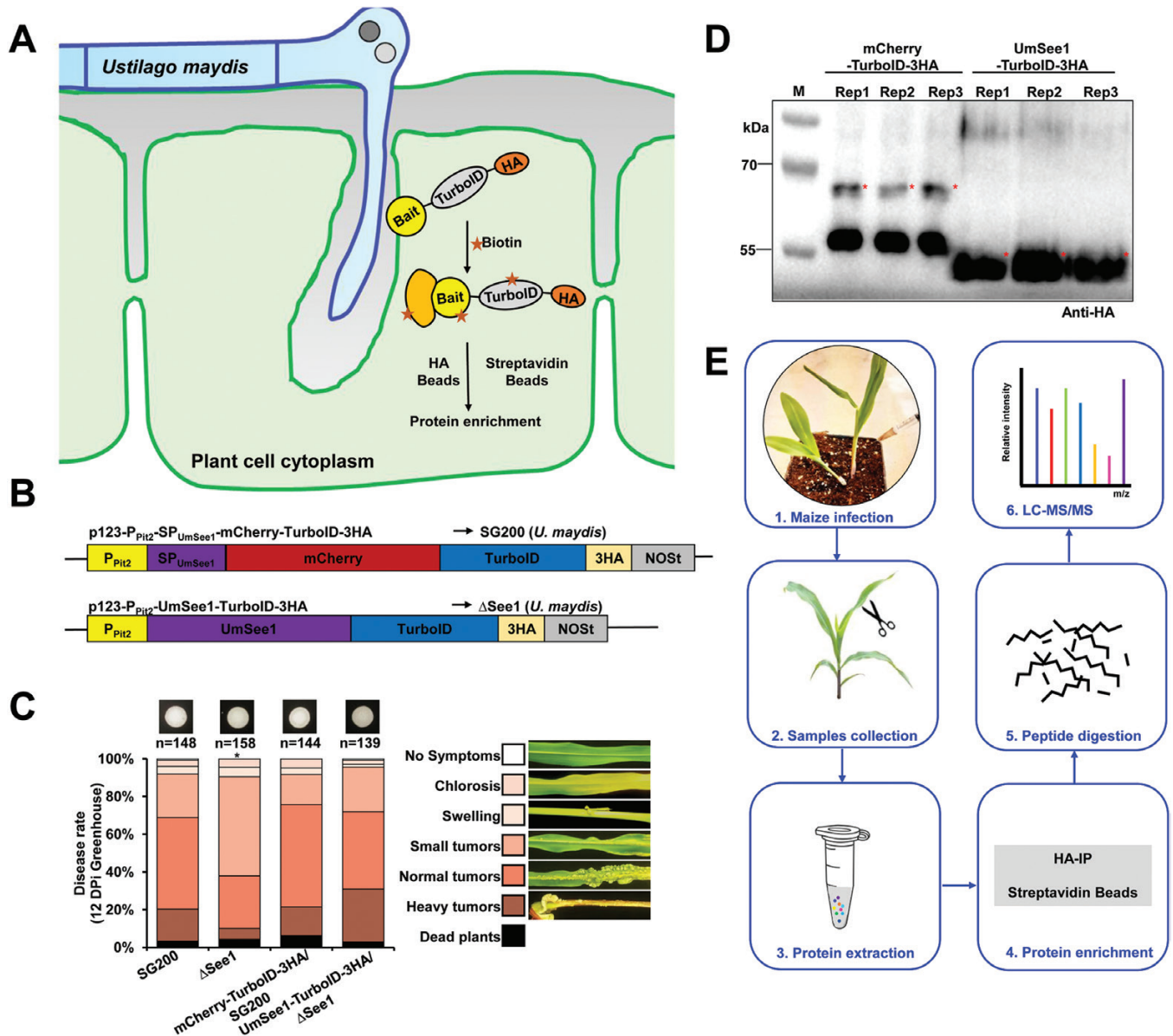


**Fig. 1.** Experimental setup for TurboID-based biotiny labeling in the *Ustilago maydis*–maize pathosystem. (A) Principle to isolate further UmSee1-interacting proteins and proteins in close proximity to UmSee1 in maize leaves via pull-down and TurboID-based proximity labeling (PL). (B) Schematic representation of the constructs used for HA-IP and Turbo-based PL. (C) Quantification of infection symptoms on EGB maize seedlings infected with *U. maydis* strains as indicated in (B) at 12 dpi. SG200, wild-type *U. maydis*; mCherry-TurboID-HA/SG200, mCherry-TurboID-3HA expressed in wild-type *U. maydis*;  $\Delta$ See1, *See1* deletion mutant; UmSee1-TurboID-3HA/ $\Delta$ See1, UmSee1-TurboID-3HA expressed in the *See1* deletion mutant. (D) Detection of mCherry–TurboID–HA and UmSee1–TurboID–HA in maize leaves upon delivery by *U. maydis*. For anti-HA immunoprecipitation, leaves were harvested at 3 dpi. Three independent replicates (Rep1–3) are shown. M, protein ladder. The asterisks represent target proteins. The expected sizes of mCherry–TurboID-3HA and UmSee1–TurboID-3HA proteins are 68.0 kDa and 54.5 kDa, respectively. (E) Overview of the workflow used to identify putative UmSee1 targets by Co-IP and TurboID-based biotiny labeling in the *U. maydis*–maize pathosystem.

that the UmSee1 interactors and proteins in close proximity to UmSee1 *in planta* belong to the ubiquitin–proteasome complex.

#### UmSee1 interacts with three UPS-related proteins

Based on the analysis described above, our data suggest an involvement of UmSee1 with proteins of the

ubiquitin–proteasome system (UPS). The previously identified UmSee1-interacting protein ZmSGT1 could be confirmed as an interactor in the HA-IP dataset. Importantly, SGT1 is a member of the SCF (Skp1/Cullin 1/F-box) complex, which associates with the ubiquitin–proteasome pathway (Cheng *et al.*, 2011).

Previous transcriptome analysis of maize leaves at the cell-type level showed that UmSee1 affects expression of

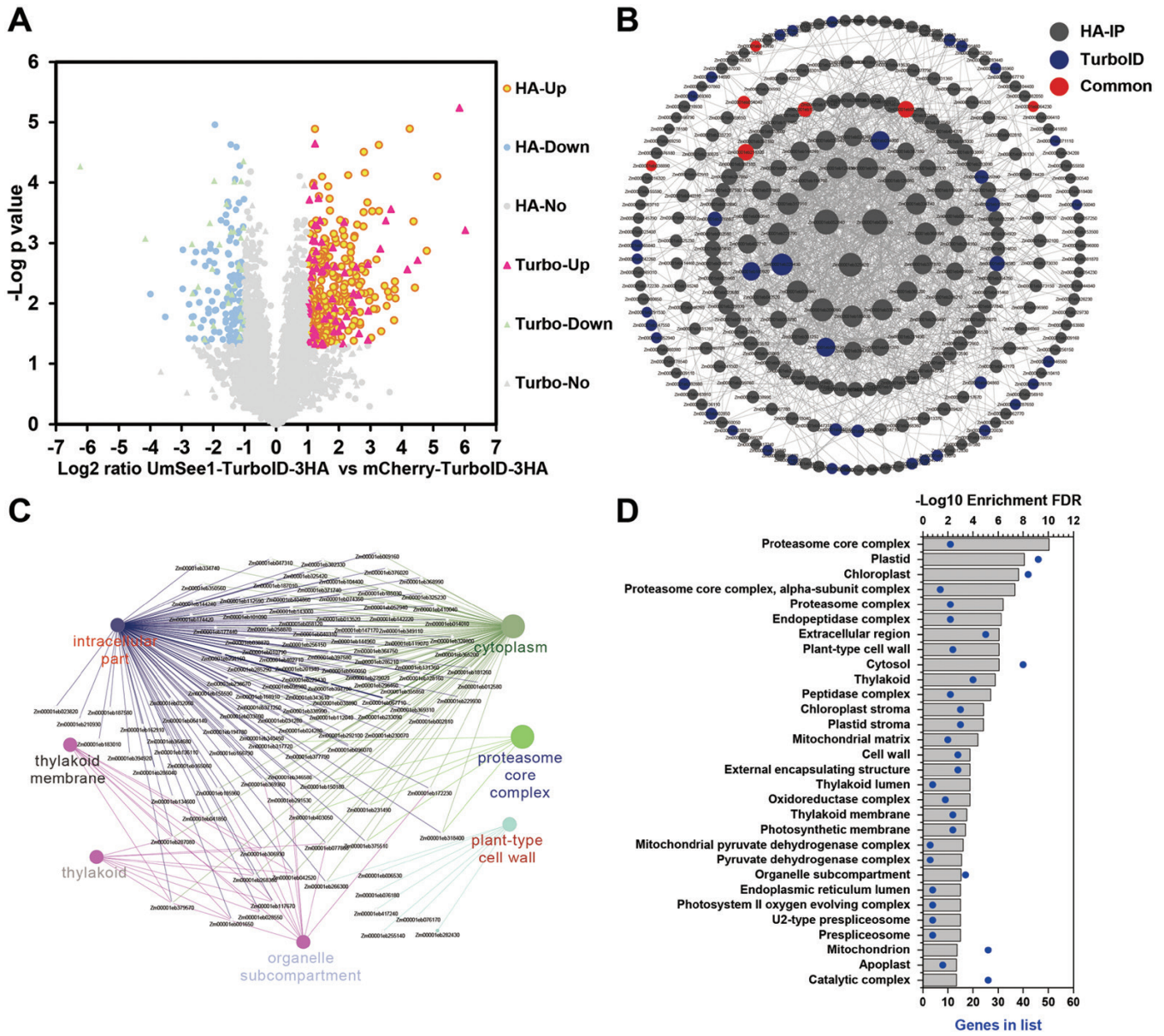


**Fig. 2.** Identification of UmSee1-interacting proteins by Co-IP and TurboID-based biotin labeling. (A) Volcano plot analysis of identified proteins from HA-IP and TurboID-based biotin labeling by LC-MS/MS. Proteins significantly enriched in UmSee1 samples are shown in the top right corner (red and yellow dots). HA-up (yellow dots), significantly enriched proteins in UmSee1 compared with mCherry samples in the HA pull-down; HA-down (blue dots), significantly enriched proteins in mCherry compared with UmSee1 samples in the HA pull-down; HA-No (green dots), no significantly enriched proteins between UmSee1 and mCherry samples in the HA pull-down dataset; Turbo-up (red triangle), significantly enriched proteins in UmSee1 compared with mCherry samples in the TurboID-based proximity labeling; Turbo-down (purple triangles), significantly enriched proteins in mCherry compared with UmSee1 samples in the TurboID-based proximity labeling; Turbo-No (green triangles), no significantly enriched proteins between UmSee1 and mCherry samples in the TurboID-based proximity labeling dataset ( $P$ -value  $< 0.05$  and  $\log_2$  fold change  $> 1$  set as significantly enriched). (B) PPI analysis of the proteins identified in UmSee1 samples using the STRING database. Proteins significantly enriched in the HA-IP and TurboID-based PL of UmSee1 samples were submitted to the STRING database, and the protein interaction network was modified and analyzed using the Cytoscape software (version 3.9.1). Edges represent protein-protein associations, including known interactions and predicted interactions (gene neighborhood, gene fusions, gene co-occurrence); the proteins identified by the different methods are marked with different colors, and the size of the shape indicates the degree of interaction. Proteins are represented by their gene ID. (C) Cluster analysis of the PPI network of the UmSee1-specific dataset by CluePedia (version 1.5.9) and ClueGo (version 2.5.9). (D) GO cellular component enrichment of the UmSee1-specific dataset using ShinyGO v0.66.

genes associated with cell reprogramming and tumor formation (Villajuana-Bonequi *et al.*, 2019). Such differentially expressed genes were primarily associated with cell cycle regulation and protein degradation, including UPS-related ubiquitin ligases and CDCs (Matei *et al.*, 2018; Villajuana-Bonequi *et al.*, 2019). We checked the previously generated cell type-specific transcriptome for differential regulation of genes encoding UmSee1-interacting proteins. This resulted in the selection of three candidates, which had been identified as differentially expressed genes and now were found by HA-IP or TurboID-based PL. We named the proteins ZmSIPs, for *Zea mays* See1-interacting proteins. Zm00001eb157120 (ZmSIP1) contains a ubiquitin-conjugating enzyme E2 motif, which was detected by both HA-IP and TurboID-based PL, but was not significantly enriched compared with the control. Zm00001eb369210 (ZmSIP2) contains a proteasome alpha type 3 domain, and was significantly enriched only in UmSee1 HA-IP samples, and Zm00001eb185960 (ZmSIP3) contains CDC48 and AAA+ domains, and was significantly enriched only in TurboID-based PL datasets. Like ZmSIP2 and ZmSIP3, ZmSIP1 is also highly expressed in mesophyll cells but not in the bundle sheath cells, as demonstrated by the cell type-specific transcriptome of maize leaves (Villajuana-Bonequi *et al.*, 2019) (Supplementary Fig. S4). Furthermore, the expression of ZmSIP2 and ZmSIP3 is affected by UmSee1 (Villajuana-Bonequi *et al.*, 2019), which might suggest that these genes could be involved in *U. maydis*-mediated tumor formation.

UmSee1 is localized in the nucleus and cytoplasm of plant cells (Redkar *et al.*, 2015a), and we therefore tested a putative subcellular co-localization of the ZmSIPs with UmSee1. The ZmSIPs were co-expressed as GFP function proteins in *N. benthamiana* leaves with UmSee1–mCherry or mCherry as the control. All genes were expressed under the control of the CaMV 35S promoter. As expected, fluorescence microscopy detected the mCherry signal for UmSee1 in the nucleus and the cytoplasm. Similarly, GFP signals could also be detected in the nucleus and the cytoplasm (Supplementary Fig. S5), suggesting that all ZmSIPs (ZmSIP1, ZmSIP2, and ZmSIP3) co-localize with UmSee1 in the same compartments upon co-overexpression *in planta*. To test for a direct PPI between UmSee1 and the ZmSIPs, a directed Y2H assay was done. The yeast transformants co-expressing each of the three ZmSIP1 proteins fused N-terminally to the GAL4AD (pGBKT7 vector) with UmSee1, or mCherry fused N-terminally to the ADH1 AD (pGADT7 vector) were selected on SD–Leu–Trp solid medium and grew in the absence of histidine (–His), which indicates physical interaction of the proteins tested. In contrast to the BD–UmSee1/AD–mCherry transformants, the transformants expressing either of the AD–ZmSIPs together with BD–UmSee1 at OD<sub>600</sub> < 1 (Fig. 3A) could grow on SD–Leu–Trp–His solid medium. The TurboID-based PL candidate interactor ZmSIP3 consistently appeared to have the lowest affinity for UmSee1 in the Y2H assays (Fig. 3A). Importantly, we obtained comparable results when UmSee1 was exchanged

with its ortholog from the maize-infecting smut species *Sporisorium reilianum*, SrSee1, in these assays (Supplementary Fig. S6). In turn, when UmSee1 was exchanged with UhSee1, the ortholog from barley-infecting *Ustilago hordei*, we could not detect any growth in the absence of histidine (Supplementary Fig. S6). This is in line with the previous finding that SrSee1, but not UhSee1 can restore the tumor formation of the UmSee1 deletion mutant (Redkar *et al.*, 2015b). We also analyzed PPIs by directed Co-IP assays. UmSee1ΔSP-6HA was co-immunoprecipitated by anti-myc immunoprecipitation of ZmSIP1-4myc, ZmSIP2-4myc, and ZmSIP3-4myc, but not with GFP-4myc, suggesting that UmSee1 interacts with ZmSIP1, ZmSIP2, and ZmSIP3 *in planta* (Fig. 3B). Again, the association of ZmSIP3 and UmSee1 appeared to be the weakest, although ZmSIP2 and ZmSIP3 protein levels were comparable in these assays. Similarly, in split-luciferase complementation imaging assays, a luminescence signal was detected when UmSee1 and all ZmSIPs were co-expressed in *N. benthamiana* leaves. We did not detect any signal in the control samples (Fig. 3C). Collectively, our data show that UmSee1 interacts with ZmSIP1, ZmSIP2, and ZmSIP3 and that the association with ZmSIP3 may be a weak and/or a transient interaction.

#### *UmSee1-interactor maize proteins are components of the ZmSGT1 complex*

SGT1 is known to regulate Skp1 in the SCF (Skp1/Cullin 1/F-box) complex, which controls the degradation of cell cycle regulators (Hermann, 2006). UmSee1 interacts with maize ZmSGT1 and can block SIPK-triggered SGT1 phosphorylation (Redkar *et al.*, 2015a). To explore the relationship between ZmSIP1, ZmSIP2, and ZmSIP3 and ZmSGT1, we tested if ZmSGT1 can also associate with the here identified ZmSIPs. Yeast transformants expressing BD–ZmSGT1 with AD–ZmSIP1 and AD–ZmSIP2 grew on the selection medium lacking histidine. Transformants co-expressing BD–ZmSGT1 and AD–ZmSIP3 grew poorly in comparison with ZmSIP1 or ZmSIP2 transformants, suggesting a stable association between UmSGT1 and ZmSIP1 or ZmSIP2, but a weak or transient association with ZmSIP3 (Fig. 4A). ZmSGT1-6HA was also co-expressed with ZmSIP1-4myc, ZmSIP2-4myc, ZmSIP3-4myc, or GFP-4myc in *N. benthamiana* leaves for Co-IP assays. ZmSGT1-6HA was precipitated at equal levels by anti-myc immunoprecipitation of ZmSIP1-4myc, ZmSIP2-4myc, and ZmSIP3-4myc but not with the GFP-4myc control (Fig. 4B), suggesting that ZmSGT1 can interplay with ZmSIP1, ZmSIP2, and ZmSIP3 *in planta*.

#### *UmSee1 interacts with components of the UPS to regulate the cell cycle*

Since ZmSIP1, ZmSIP2, and ZmSIP3 are all proteins related to the UPS, we performed an ABPP assay to explore whether

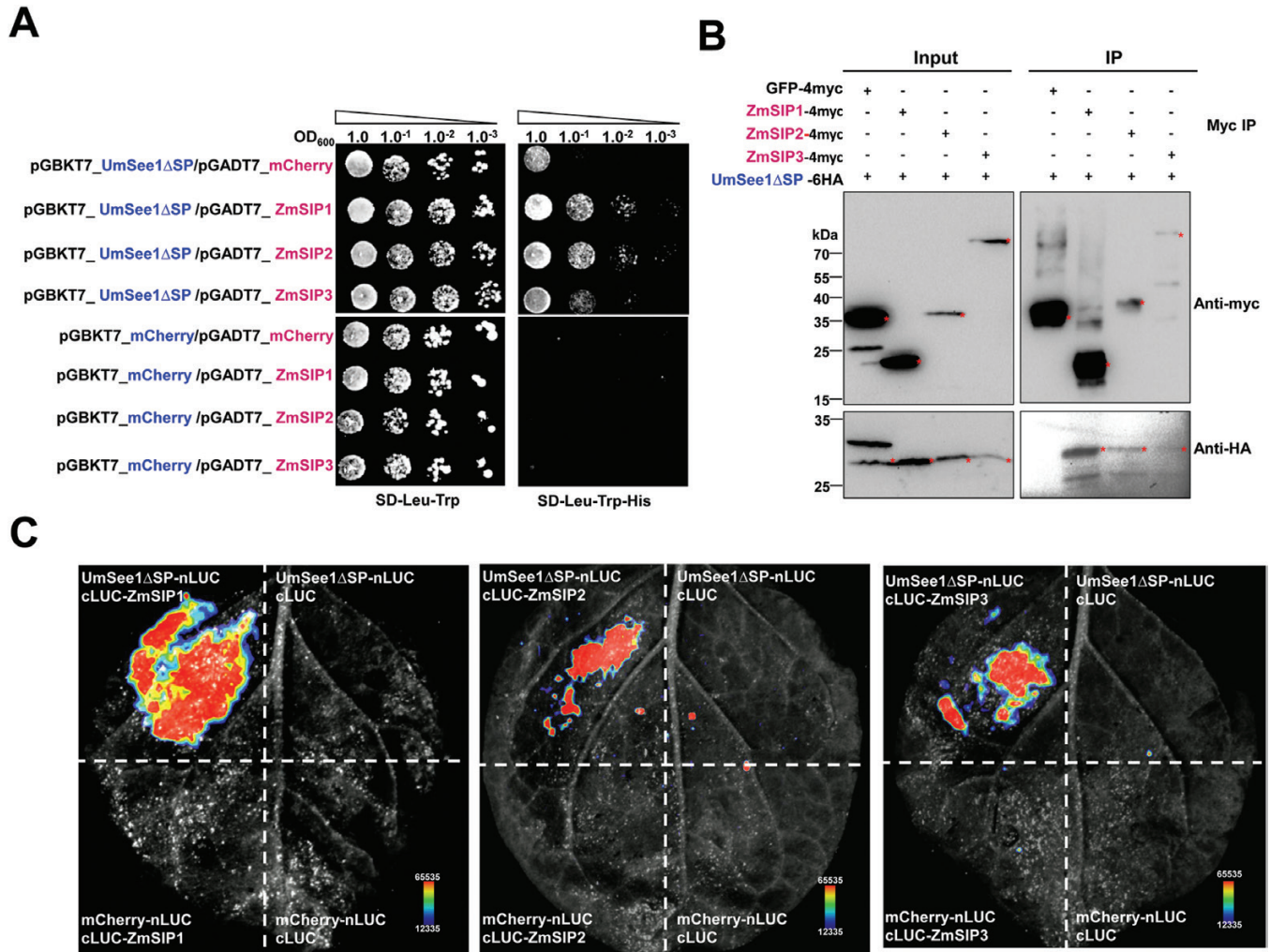


**Fig. 3.** Three identified proteins enriched in theUmSee1 dataset interact with UmSee1 in one-to-one interaction assays. (A) Y2H assay of UmSee1 and three putative UmSee1 interaction partners (ZmSIPs). The yeast strain AH109 was co-transformed with mCherry or UmSee1ΔSP (UmSee1 without signal peptide) and the constructs of ZmSIPs (ZmSIP1, ZmSIP2, and ZmSIP3). A drop-out assay of a dilution series of the double transformants was carried out in the presence (SD-Trp-Leu) and absence (SD-Trp-Leu-His) of histidine. Yeast growth in the absence of histidine suggests the interaction of proteins. Pictures of three independent experiments were taken 5 d after plating. (B) Co-IP assays of UmSee1 and the three ZmSIPs. *N. benthamiana* leaves were transiently transformed with the constructs encoding UmSee1ΔSP-6HA and ZmSIPs-4myc or GFP-4Myc. Leaves were harvested 3 d post-*Agrobacterium*-mediated transformation for protein extraction. Anti-myc immunoprecipitation (IP) was performed and total extracts and IP proteins were detected by western blot analysis using anti-HA and anti-myc. The expected sizes of GFP-4myc, ZmSIP1-4myc, ZmSIP2-4myc, ZmSIP3-4myc, and UmSee1ΔSP-6HA proteins are 31.9, 20.5, 32.2, 86.1, and 26.4 kDa, respectively. (C) Split-luciferase assay of UmSee1 and the three ZmSIPs. *N. benthamiana* plants were transiently transformed with constructs of UmSee1ΔSP-nLUC or mCherry-nLUC and cLUC-ZmSIPs (ZmSIP1, ZmSIP2, and ZmSIP3) or cLUC as indicated. Leaves were harvested 2 d post-*Agrobacterium*-mediated transformation and treated with 1 mM D-luciferin for 10 min in the dark. Shown are representative pictures of luminescence signals from three independent biological replicates. Images were detected by the CCD imaging system (ChemiDoc, Bio-Rad).

heterologously expressed UmSee1 affects maize proteasome activity. For this, total proteins extracted from maize leaves were mixed with BSA or recombinant UmSee1 without SP (6His-UmSee1ΔSP) obtained from *E. coli*. Samples were pre-incubated in the presence or absence of the proteasome inhibitor epoxomicin and labeled with the specific proteasome activity-based probe MVB072 (Kolodziejek *et al.*, 2011). MVB072 binds covalently and irreversibly to the active site of the catalytic proteasome subunits beta-1, beta-2, and beta-5, and contains a

bodipy tag for fluorescent detection and a biotin tag for affinity purification (Kolodziejek *et al.*, 2011). Proteasome-specific signals were observed at ~26 kDa, and those signals were inhibited in the presence of epoxomicin (Fig. 5A). We quantified ABPP signals to determine whether proteasome activity was enhanced in the presence of UmSee1. The percentage of proteasome activity was plotted and compared with the BSA control. We detected significantly enhanced activity of the maize proteasome in the presence of recombinant 6His-UmSee1ΔSP

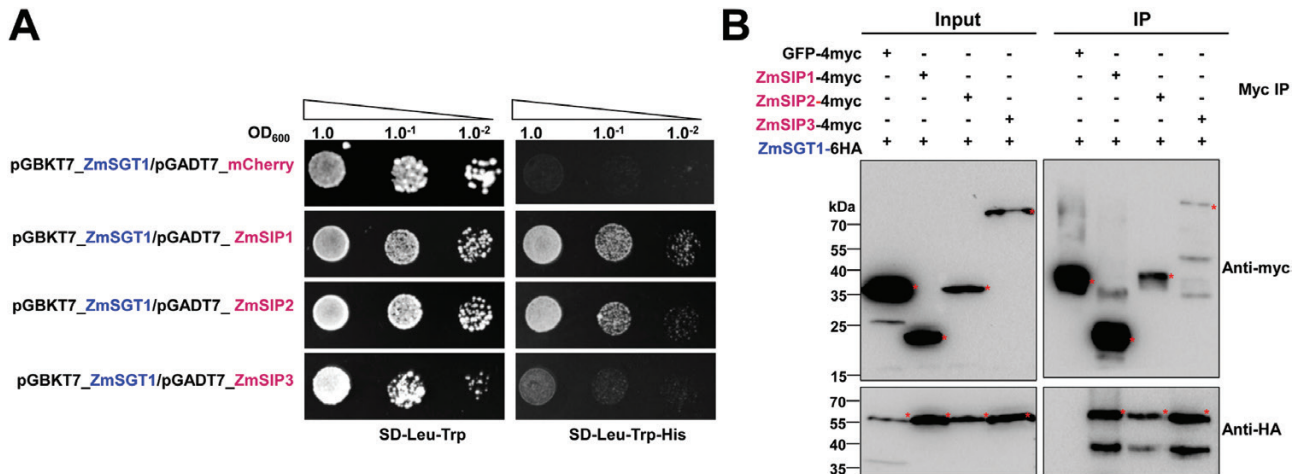


**Fig. 4.** Three identified UmSee1 interactors are associated with the ZmSGT1-interacting protein complex. (A) Y2H assays of SGT1 and the three ZmSIPs. The yeast strain AH109 was co-transformed with ZmSGT1 and the three ZmSIPs, ZmSIP1, ZmSIP2, and ZmSIP3, or mCherry as a negative control. A drop-out assay of dilution series of the double transformants was carried out in the presence (SD-Trp-Leu) and absence (SD-Trp-Leu-His) of histidine. Yeast growth in the absence of histidine suggests the interaction of proteins. Shown are representative pictures of three independent biological experiments taken 5 d after drop-out plating. (B) Co-IP assays of ZmSGT1 and the ZmSIPs. *N. benthamiana* leaves were transiently transformed with the ZmSGT1-6HA and ZmSIPs (ZmSIP1, ZmSIP2, and ZmSIP3)-4myc constructs. Leaves were harvested 3 d post-*Agrobacterium*-mediated transformation for protein extraction. Anti-myc immunoprecipitation (IP) was performed and total extracts and IP proteins were detected by western blot analysis using anti-HA and anti-myc. The expected sizes of GFP-4myc, ZmSIP1-4myc, ZmSIP2-4myc, ZmSIP3-4myc, and ZmSGT1-6HA proteins are 31.9, 20.5, 32.2, 86.1, and 53.6 kDa, respectively.

in comparison with the control sample (Fig. 5A, B). Thus, addition of recombinant 6His-UmSee1 enhances *in vitro* proteasome activity of maize. To explore the effect of UmSee1 on the ubiquitination of maize proteins, 7-day-old maize leaves were infected with *U. maydis* strains SG200 or SG200ΔSee1. Total extracted proteins were detected via western blot using an  $\alpha$ -ubiquitin antibody. We consistently detected stronger ubiquitination in SG200-infected leaves when compared with SG200ΔSee1-infected leaves, suggesting that UmSee1, directly or indirectly, increases the ubiquitination of maize proteins during infection (Fig. 5C). Interestingly, the expression pattern of the proteasome alpha subunit ZmSIP2 is down-regulated in SG200ΔSee1-infected leaves in comparison with SG200 infection, but the expression of the catalytic beta-1 proteasome subunit PBA1 (GRMZM2G1775) does not change during infection (Supplementary Fig. S4) (Villajuana-Bonequi *et al.*, 2019), suggesting a normal core proteasome activity but a somehow disrupted structure of the 20S barrel in the absence of UmSee1. How could one then connect UmSee1-dependent proteasomal activity to its role in the activation of plant cell cycle? A possible link could be ZmSIP3, which contains CDC48 and AAA+ domains related to cell cycle regulation. The protein stability of ZmSIP3 may be important for cell cycle regulation. To explore if the UmSee1-driven effects on proteasome activity and ubiquitination alter the stability of ZmSIP3, we performed a protein degradation analysis of ZmSIP3 in the presence of UmSee1ΔSP-mCherry-6HA, as well as an mCherry-6HA control (Fig. 5D). For this, ZmSIP3-4myc, mCherry-6HA, and UmSee1ΔSP-mCherry-6HA were separately expressed in *N. benthamiana* leaves using

*Agrobacterium*-mediated transformation. ZmSIP3-4myc protein extracts were supplemented with increasing concentrations of mCherry-6HA or UmSee1ΔSP-mCherry-6HA containing extracts in the presence or absence of the proteasome inhibitor MG132. Samples were incubated at 28 °C for 45 min, and the amount of ZmSIP3-4myc was detected by western blot using anti-myc antibodies. ZmSIP3-4myc protein levels decreased with increasing UmSee1ΔSP-mCherry-6HA concentrations, and this degradation process was inhibited by the addition of MG132. This decrease of ZmSIP3-4myc was seen significantly less when UmSee1ΔSP-mCherry-6HA was exchanged by mCherry-6HA. These data indicate an enhanced proteasome-mediated degradation of ZmSIP3 in the presence of UmSee1. To test if degradation in the presence of UmSee1 is specific for ZmSIP3, we also performed the protein degradation analysis for ZmSIP1 and ZmSIP2. However, in both cases, we did not observe significant protein degradation in the presence of UmSee1 (Supplementary Fig. S7). Collectively, our results suggest a possible UPS regulatory network modulated by UmSee1 that facilitates cell cycle progression and may promote tumorigenesis (Fig. 5E).

## Discussion

### Combination of AP-MS and TurboID-based PL identifies the UmSee1 interaction network

Plant pathogens target host proteins with secreted effectors to facilitate infection. Thus, the identification of effector targets helps to us understand both microbial virulence strategies



and mechanisms of plant immunity. Conventional approaches for identifying protein interactors are Y2H library screenings and affinity purification followed by mass spectrometry (AP-MS) (Paraoan *et al.*, 2020; Woloschuk *et al.*, 2020). ZmSGT1 was identified as an interactor of UmSee1 via a Y2H library screen, and this interaction was confirmed by AP-MS (Redkar *et al.*, 2015a). However, this strategy probably fails to explore complex effector–target interaction networks, which can be dynamic and transient in nature. Plant pathogen effectors can target multiple host proteins to effectively disrupt a single or various biological pathways and promote virulence (Khan *et al.*, 2018). For example, *Pseudomonas syringae* effector HopM1 (HopPtoM) is required for full virulence by targeting MIN7 (ARF-GEF), MIN10 (GRF10), UPL1, UPL3, and ECM29 proteins in Arabidopsis (Toruño *et al.*, 2016; Üstün *et al.*, 2016; Khan *et al.*, 2018). Another example is the effector AvrPiZ-t from *Magnaporthe oryzae*, which targets Nup98 homolog APIP12 and the E3 ligases APIP6 and APIP10 in rice to promote infection (Park *et al.*, 2012, 2016; Tang *et al.*, 2017).

Enzyme-catalyzed proximity labeling approaches have been increasingly used as an alternative screening method for capturing weak or transient protein interactions by labeling the neighboring proteins with biotin (Gingras *et al.*, 2019). TurboID-based PL is ideal for low affinity, transient interactions, and proteins insoluble under native extraction conditions (Zhang *et al.*, 2019; Melkonian *et al.*, 2022). The components of regulators and many subcellular organelles involved in various cellular processes have been identified by TurboID-based PL in mammalian cells and some model plants, but it has not yet been used in the context of fungal pathogens.

In this study, we established TurboID-based PL for exploiting the so far unidentified interactors of the organ-specific effector UmSee1 in the *U. maydis*–maize pathosystem (Fig. 1; Supplementary Fig. S1). Combination of all putative UmSee1-interacting proteins identified by Co-IP and TurboID-based PL revealed that components of the UPS were enriched in the UmSee1 interaction network (Fig. 2). Three UPS-related proteins (ZmSIP1, ZmSIP2, and ZmSIP3) were confirmed to interact with UmSee1 (Fig. 3). ZmSIP1 was found to contain a ubiquitin-conjugating enzyme E2 motif, catalytic (UBCc) domain, suggesting that ZmSIP1 in maize may perform as an E2 ubiquitin-conjugating enzyme. E2 enzymes have been found to regulate the processing and topology of polyubiquitin chain formation and other modifications, thus determining the destiny of the modified proteins (Zhou *et al.*, 2017). For example, *P. sojae* effector Avr1d functions as an E2 competitor and inhibits ubiquitination activity of the U-box-type E3 ligase GmPUB13 to facilitate infection (Misas-Villamil *et al.*, 2013; Lin *et al.*, 2021). The interaction of UmSee1 and ZmSIP1 may be linked to the proteasome alpha subunit ZmSIP2 and the increased ubiquitination observed upon *U. maydis* infection, but the molecular mechanism behind this phenotype needs to be further investigated. ZmSIP2 contains a proteasome alpha type 3 domain,

which is part of the central core 20S proteasome containing the catalytic subunits responsible for protein degradation in the cytoplasm and nucleus. The plant proteasome is a key regulator of protein stability and has been identified as a hub in plant immunity since it is targeted by multiple bacterial and fungal effector molecules, such as SylA and HopZ4 from *P. syringae* or higginsianin B from the fungus *Colletotrichum higginsianum* that bind and inhibit proteasome activity, suppressing plant immunity (Misas-Villamil *et al.*, 2013; Üstün *et al.*, 2014; Dallery *et al.*, 2020). The interaction of UmSee1 and ZmSIP2 may be linked to the UmSee1-mediated proteasome activation. Interestingly, ZmSIP1 and ZmSIP2 directly interacted with ZmSGT1, and ZmSIP3 is the weakest interactor of UmSee1 and ZmSGT1, indicating that ZmSIP1 and ZmSIP2 may regulate or belong to the SGT1–SCF complex (Fig. 4). Further investigation is needed to fully understand the molecular mechanism.

#### Towards an understanding of effector-mediated modulation of cell cycle control

UmSee1 interacts with and alters the function of UPS components. The observed UmSee1-mediated increase in proteasome activity suggests that this effector affects proteasome function or regulation (Fig. 5A), although it is not yet clear if the *in vitro* proteasomal activation observed is specific for UmSee1, or if it is a consequence of UmSee1 degradation where UmSee1 is used as a substrate. If UmSee1 specifically activates proteasomal degradation, one would expect an increased degradation efficiency of certain proteins. In this context, it is important that essential cell cycle regulators are associated with the UPS, and that the UPS regulates cell growth and proliferation boundaries between the G<sub>1</sub> and S phase (Bashir *et al.*, 2004). The UmSee1 interactor ZmSIP3 is a CDC48 domain-containing protein [i.e. a conserved AAA+ (ATPases Associated with diverse cellular Activities) ATPase] which are enzymes known to be involved in cell cycle control, cytokinesis, and cell proliferation (Stolz *et al.*, 2011). CDC48 was first identified in yeast, where it is important for cell cycle progression (Buchberger, 2013). In plants, CDC48 is involved in multiple processes, such as germination, reproduction, tissue differentiation, and immune response. For example, *A. thaliana* CDC48A is involved in embryo growth and the degradation of immune receptors (Li *et al.*, 2022). Thus, the increase of UPS-mediated degradation of ZmSIP3 in the presence of UmSee1 might provide a hint as to how *U. maydis* triggers cell proliferation in the host. Based on our findings, a possible scenario (Fig. 5E) is that UmSee1 interferes with components of the SGT1–SCF complex to potentiate UPS activity. This leads to an increased degradation of cell cycle regulators, including CDC48 protein, which promotes the activation of cell cycle progression observed in *U. maydis*-induced tumorigenesis. In future studies, this working model can be tested to dissect the molecular interplay between the UPS and the tumor-inducing function of UmSee1.

In summary, we have established TurboID-based PL in combination with Co-IP followed by LC-MS/MS to identify a protein interaction network of the UmSee1 effector. This approach is widely applicable, in particular for establishing interaction networks of effectors which interfere with complex cellular processes. Insight into protein networks and their modulation by effectors will increase our mechanistic understanding of microbial pathogenesis. Moreover, it provides new starting points for the biochemical and structural elucidation of effector–target interactions and therefore holds a strong potential to establish new strategies for plant disease control and crop improvement.

## Supplementary data

The following supplementary data are available at [JXB online](#).

Fig. S1. UmSee1-interacting protein enrichment by TurboID-based biotin labeling.

Fig. S2. Protein–protein interaction (PPI) analysis of proteins that were specifically identified in UmSee1 samples.

Fig. S3. Gene Ontology (GO) analysis of proteins that were specifically identified in UmSee1 samples.

Fig. S4. Identified ZmSIPs (ZmSIP1, ZmSIP2, and ZmSIP3).

Fig. S5. Subcellular localization of ZmSIPs and UmSee1 upon expression in *Nicotiana benthamiana*.

Fig. S6. Y2H assays involving SrSee1 and UhSee1 and the ZmSIPs.

Fig. S7. *In vitro* protein degradation analysis of ZmSIP1 and ZmSIP2.

Table S1. Primers used in this study.

Table S2. Fungal strains used in this study.

Table S3. Quantification of infection symptoms on maize seedlings at 12 dpi.

Table S4. Mass spectrometry data of UmSee1.

Table S5. List of identified UmSee1-interacting proteins.

## Acknowledgements

We would like to thank Weiliang Zuo for helpful discussion and suggestions, Ute Meyer for technical support, Anne Harzen for MS sample processing, Katharina Melkonian for helpful practical advice on the TurboID-based PL approach, and Hermen Overkleeft for providing the MVB072 probe.

## Author contributions

WS, IMLS, JCMV, and GD: design; WS, SCS, HN, JCMV, IMLS, and GD: performing the experiments and data analysis; WS, JCMV, IMLS, and GD: writing with contributions from all the other authors.

## Conflict of interest

The authors declare no conflicts of interest.

## Funding

This work was funded by the European Research Council under the European Union's Horizon 2020 research and innovation program (consolidator grant conVIRgens, ID 771035) to GD, the Deutsche Forschungsgemeinschaft (DFG) Emmy Noether Programme (SA 4093/1-1) to IMLS, and the Daimler and Benz Foundation (to IMLS). HN is supported by the Max Planck Society and is grateful for funding by the DFG (NA 946/1-1). We acknowledge funding from the Cluster of Excellence on Plant Sciences (CEPLAS) funded by the DFG (German Research Foundation) under Germany's Excellence Strategy—EXC 2048/1—Project ID: 390686111 to GD, JCMV, and IMLS.

## Data availability

The data supporting the findings of this study are available within the paper and its supplementary data. The mass spectrometry proteomics data are available via ProteomeXchange with identifier PXD040939.

## References

- Bashir T, Dorrello NV, Amador V, Guardavaccaro D, Pagano M.** 2004. Control of the SCFSkp2–Cks1 ubiquitin ligase by the APC/CCdh1 ubiquitin ligase. *Nature* **428**, 190–193.
- Bindea G, Galon J, Mlecnik B.** 2013. CluePedia Cytoscape plugin: pathway insights using integrated experimental and *in silico* data. *Bioinformatics* **29**, 661–663.
- Bindea G, Mlecnik B, Hackl H, Charoentong P, Tosolini M, Kirilovsky A, Fridman WH, Pages F, Trajanoski Z, Galon J.** 2009. ClueGO: a Cytoscape plug-in to decipher functionally grouped gene ontology and pathway annotation networks. *Bioinformatics* **25**, 1091–1093.
- Bindics J, Khan M, Uhse S, et al.** 2022. Many ways to TOPLESS—manipulation of plant auxin signalling by a cluster of fungal effectors. *New Phytologist* **236**, 1455–1470.
- Branon TC, Bosch JA, Sanchez AD, Udeshi ND, Svinkina T, Carr SA, Feldman JL, Perrimon N, Ting AY.** 2018. Efficient proximity labeling in living cells and organisms with TurboID. *Nature Biotechnology* **36**, 880–887.
- Buchberger A.** 2013. Roles of Cdc48 in regulated protein degradation in yeast. *Subcellular Biochemistry* **66**, 195–222.
- Cheng YT, Li YZ, Huang SA, Huang Y, Dong XN, Zhang YL, Li X.** 2011. Stability of plant immune-receptor resistance proteins is controlled by SKP1–CULLIN1–F-box (SCF)-mediated protein degradation. *Proceedings of the National Academy of Sciences, USA* **108**, 14694–14699.
- Conlan B, Stoll T, Gorman JJ, Saur I, Rathjen JP.** 2018. Development of a rapid in planta BioID system as a probe for plasma membrane-associated immunity proteins. *Frontiers in Plant Science* **9**, 1882.
- Cox J, Mann M.** 2008. MaxQuant enables high peptide identification rates, individualized ppb-range mass accuracies and proteome-wide protein quantification. *Nature Biotechnology* **26**, 1367–1372.
- Dallery JF, Zimmer M, Halder V, et al.** 2020. Inhibition of jasmonate-mediated plant defences by the fungal metabolite higginsianin B. *Journal of Experimental Botany* **71**, 2910–2921.
- Dang F, Nie L, Wei W.** 2021. Ubiquitin signaling in cell cycle control and tumorigenesis. *Cell Death & Differentiation* **28**, 427–438.
- Darino M, Chia KS, Marques J, et al.** 2021. *Ustilago maydis* effector Jsi1 interacts with Topless corepressor, hijacking plant jasmonate/ethylene signaling. *New Phytologist* **229**, 3393–3407.
- Dielen AS, Badaoui S, Candresse T, German-Retana S.** 2010. The ubiquitin/26S proteasome system in plant–pathogen interactions: a never-ending hide-and-seek game. *Molecular Plant Pathology* **11**, 293–308.

- Djamei A, Schipper K, Rabe F, et al.** 2011. Metabolic priming by a secreted fungal effector. *Nature* **478**, 395–398.
- Dodds PN, Rathjen JP.** 2010. Plant immunity: towards an integrated view of plant–pathogen interactions. *Nature Reviews. Genetics* **11**, 539–548.
- Doehlemann G, Reissmann S, Aßmann D, Fleckenstein M, Kahmann R.** 2011. Two linked genes encoding a secreted effector and a membrane protein are essential for *Ustilago maydis*-induced tumour formation. *Molecular Microbiology* **81**, 751–766.
- Doehlemann G, van der Linde K, Amann D, Schwammbach D, Hof A, Mohanty A, Jackson D, Kahmann R.** 2009. Pep1, a secreted effector protein of *Ustilago maydis*, is required for successful invasion of plant cells. *PLoS Pathogens* **5**, e1000290.
- Doehlemann G, Wahl R, Horst RJ, et al.** 2008. Reprogramming a maize plant: transcriptional and metabolic changes induced by the fungal biotroph *Ustilago maydis*. *The Plant Journal* **56**, 181–195.
- Fisher MC, Gow NA, Gurr SJ.** 2016. Tackling emerging fungal threats to animal health, food security and ecosystem resilience. *Philosophical Transactions of the Royal Society B: Biological Sciences* **371**, 20160332.
- Ge SX, Jung D, Yao R.** 2020. ShinyGO: a graphical gene-set enrichment tool for animals and plants. *Bioinformatics* **36**, 2628–2629.
- Gingras AC, Abe KT, Raught B.** 2019. Getting to know the neighborhood: using proximity-dependent biotinylation to characterize protein complexes and map organelles. *Current Opinion in Chemical Biology* **48**, 44–54.
- Herland D.** 2006. F-box proteins: more than baits for the SCF? *Cell Division* **1**, 1–6.
- Hogenhout SA, Van der Hoorn RAL, Terauchi R, Kamoun S.** 2009. Emerging concepts in effector biology of plant-associated organisms. *Molecular Plant-Microbe Interactions* **22**, 115–122.
- Holzer E, Rumpf-Kienzl C, Falk S, Dammermann A.** 2022. A modified TurboID approach identifies tissue-specific centriolar components in *C. elegans*. *PLoS Genetics* **18**, e1010150.
- Jacobs C, Domian IJ, Maddock JR, Shapiro L.** 1999. Cell cycle-dependent polar localization of an essential bacterial histidine kinase that controls DNA replication and cell division. *Cell* **97**, 111–120.
- Kahmann R, Kamper J.** 2004. *Ustilago maydis*: how its biology relates to pathogenic development. *New Phytologist* **164**, 31–42.
- Kämper J.** 2004. A PCR-based system for highly efficient generation of gene replacement mutants in *Ustilago maydis*. *Molecular Genetics and Genomics* **271**, 103–110.
- Kämper J, Kahmann R, Bölker M, et al.** 2006. Insights from the genome of the biotrophic fungal plant pathogen *Ustilago maydis*. *Nature* **444**, 97–101.
- Khan M, Seto D, Subramaniam R, Desveaux D.** 2018. Oh, the places they'll go! A survey of phytopathogen effectors and their host targets. *The Plant Journal* **93**, 651–663.
- Kitagawa K, Skowrya D, Elledge SJ, Harper JW, Hieter P.** 1999. SGT1 encodes an essential component of the yeast kinetochore assembly pathway and a novel subunit of the SCF ubiquitin ligase complex. *Molecular Cell* **4**, 21–33.
- Kolodziejek I, Misas-Villamil JC, Kaschani F, et al.** 2011. Proteasome activity imaging and profiling characterizes bacterial effector syringolin A. *Plant Physiology* **155**, 477–489.
- Lanver D, Tollot M, Schweizer G, et al.** 2017. *Ustilago maydis* effectors and their impact on virulence. *Nature Reviews. Microbiology* **15**, 409–421.
- Larochelle M, Bergeron D, Arcand B, Bachand F.** 2019. Proximity-dependent biotinylation mediated by TurboID to identify protein–protein interaction networks in yeast. *Journal of Cell Science* **132**, jcs232249.
- Li J, Yuan J, Li Y, Sun H, Ma T, Huai J, Yang W, Zhang W, Lin R.** 2022. The CDC48 complex mediates ubiquitin-dependent degradation of intra-chloroplast proteins in plants. *Cell Reports* **39**, 110664.
- Li Y, Sousa R.** 2012. Expression and purification of *E. coli* BirA biotin ligase for in vitro biotinylation. *Protein Expression and Purification* **82**, 162–167.
- Lin Y, Hu Q, Zhou J, et al.** 2021. *Phytophthora sojae* effector Avr1d functions as an E2 competitor and inhibits ubiquitination activity of GmPUB13 to facilitate infection. *Proceedings of the National Academy of Sciences, USA* **118**, e2018312118.
- Liu L, Zhang Y, Tang S, Zhao Q, Zhang Z, Zhang H, Dong L, Guo H, Xie Q.** 2010. An efficient system to detect protein ubiquitination by agroinfiltration in *Nicotiana benthamiana*. *The Plant Journal* **61**, 893–903.
- Mair A, Xu SL, Branon TC, Ting AY, Bergmann DC.** 2019. Proximity labeling of protein complexes and cell-type-specific organellar proteomes in Arabidopsis enabled by TurboID. *eLife* **8**, e47864.
- Matei A, Ernst C, Günl M, Thiele B, Altmüller J, Walbot V, Usadel B, Doehlemann G.** 2018. How to make a tumour: cell type specific dissection of *Ustilago maydis*-induced tumour development in maize leaves. *New Phytologist* **217**, 1681–1695.
- Melkonian K, Stolze SC, Harzen A, Nakagami H.** 2022. miniTurbo-based interactomics of two plasma membrane-localized SNARE proteins in *Marchantia polymorpha*. *New Phytologist* **235**, 786–800.
- Misas-Villamil JC, Kolodziejek I, Crabill E, Kaschani F, Niessen S, Shindo T, Kaiser M, Alfano JR, van der Hoorn RA.** 2013. *Pseudomonas syringae* pv. *syringae* uses proteasome inhibitor syringolin A to colonize from wound infection sites. *PLoS Pathogens* **9**, e1003281.
- Misas-Villamil JC, van der Burgh AM, Grosse-Holz F, et al.** 2017. Subunit-selective proteasome activity profiling uncovers uncoupled proteasome subunit activities during bacterial infections. *The Plant Journal* **90**, 418–430.
- Misas Villamil JC, Mueller AN, Demir F, et al.** 2019. A fungal substrate mimicking molecule suppresses plant immunity via an inter-kingdom conserved motif. *Nature Communications* **10**, 1–15.
- Mlecnik B, Galon J, Bindea G.** 2019. Automated exploration of gene ontology term and pathway networks with ClueGO-REST. *Bioinformatics* **35**, 3864–3866.
- Mueller AN, Ziemann S, Treitschke S, Assmann D, Doehlemann G.** 2013. Compatibility in the *Ustilago maydis*–maize interaction requires inhibition of host cysteine proteases by the fungal effector Pit2. *PLoS Pathogens* **9**, e1003177.
- Navarrete F, Grujic N, Stirnberg A, et al.** 2021. The Pleiades are a cluster of fungal effectors that inhibit host defenses. *PLoS Pathogens* **17**, e1009641.
- Ngounou Wetie AG, Sokolowska I, Woods AG, Roy U, Deinhardt K, Darie CC.** 2014. Protein–protein interactions: switch from classical methods to proteomics and bioinformatics-based approaches. *Cellular and Molecular Life Sciences* **71**, 205–228.
- Paiano A, Margiotta A, De Luca M, Bucci C.** 2019. Yeast two-hybrid assay to identify interacting proteins. *Current Protocols in Protein Science* **95**, e70.
- Paraoan LI, Sharif U, Kelly L, Carlsson E.** 2020. Intracellular RPE interactome analysis of protein variants associated with AMD by affinity purification mass spectrometry. *Investigative Ophthalmology & Visual Science* **61**, 3688.
- Park CH, Chen SB, Shirsekar G, et al.** 2012. The *Magnaporthe oryzae* effector AvrPiz-t targets the RING E3 ubiquitin ligase APIP6 to suppress pathogen-associated molecular pattern-triggered immunity in rice. *The Plant Cell* **24**, 4748–4762.
- Park CH, Shirsekar G, Bellizzi M, et al.** 2016. The E3 ligase APIP10 connects the effector AvrPiz-t to the NLR receptor Piz-t in rice. *PLoS Pathogens* **12**, e1005529.
- Perez-Riverol Y, Bai J, Bandla C, et al.** 2022. The PRIDE database resources in 2022: a hub for mass spectrometry-based proteomics evidences. *Nucleic Acids Research* **50**, D543–D552.
- Rappsilber J, Ishihama Y, Mann M.** 2003. Stop and go extraction tips for matrix-assisted laser desorption/ionization, nanoelectrospray, and LC/MS sample pretreatment in proteomics. *Analytical Chemistry* **75**, 663–670.
- Redkar A, Hoser R, Schilling L, Zechmann B, Krzymowska M, Walbot V, Doehlemann G.** 2015a. A secreted effector protein of *Ustilago maydis* guides maize leaf cells to form tumors. *The Plant Cell* **27**, 1332–1351.

- Redkar A, Villajuana-Bonequi M, Doehlemann G.** 2015b. Conservation of the *Ustilago maydis* effector See1 in related smuts. *Plant Signaling & Behavior* **10**, e1086855.
- Saado I, Chia KS, Betz R, et al.** 2022. Effector-mediated relocation of a maize lipoxygenase protein triggers susceptibility to *Ustilago maydis*. *The Plant Cell* **34**, 2785–2805.
- Schneider CA, Rasband WS, Eliceiri KW.** 2012. NIH Image to ImageJ: 25 years of image analysis. *Nature Methods* **9**, 671–675.
- Sciuto MR, Coppola V, Iannolo G, De Maria R, Haas TL.** 2019. Two-step co-immunoprecipitation (TIP). *Current Protocols in Molecular Biology* **125**, e80.
- Shannon P, Markiel A, Ozier O, Baliga NS, Wang JT, Ramage D, Amin N, Schwikowski B, Ideker T.** 2003. Cytoscape: a software environment for integrated models of biomolecular interaction networks. *Genome Research* **13**, 2498–2504.
- Skibbe DS, Doehlemann G, Fernandes J, Walbot V.** 2010. Maize tumors caused by *Ustilago maydis* require organ-specific genes in host and pathogen. *Science* **328**, 89–92.
- Stayton PS, Freitag S, Klumb LA, et al.** 1999. Streptavidin–biotin binding energetics. *Biomolecular Engineering* **16**, 39–44.
- Stolz A, Hilt W, Buchberger A, Wolf DH.** 2011. Cdc48: a power machine in protein degradation. *Trends in Biochemical Sciences* **36**, 515–523.
- Szklarczyk D, Gable AL, Nastou KC, et al.** 2021. The STRING database in 2021: customizable protein–protein networks, and functional characterization of user-uploaded gene/measurement sets. *Nucleic Acids Research* **49**, D605–D612.
- Tanaka S, Brefort T, Neidig N, Djamei A, Kahnt J, Vermerris W, Koenig S, Feussner K, Feussner I, Kahmann R.** 2014. A secreted *Ustilago maydis* effector promotes virulence by targeting anthocyanin biosynthesis in maize. *eLife* **3**, e01355.
- Tang MZ, Ning YS, Shu XL, Dong B, Zhang HY, Wu DX, Wang H, Wang GL, Zhou B.** 2017. The Nup98 homolog APIP12 targeted by the effector AvrPiz-t is involved in rice basal resistance against *Magnaporthe oryzae*. *Rice* **10**, 1–11.
- Toruño TY, Stergiopoulos I, Coaker G.** 2016. Plant-pathogen effectors: cellular probes interfering with plant defenses in spatial and temporal manners. *Annual Review of Phytopathology* **54**, 419–441.
- Tyanova S, Temu T, Cox J.** 2016. The MaxQuant computational platform for mass spectrometry-based shotgun proteomics. *Nature Protocols* **11**, 2301–2319.
- Üstün S, König P, Guttman DS, Börnke F.** 2014. HopZ4 from *Pseudomonas syringae*, a member of the HopZ type III effector family from the YopJ superfamily, inhibits the proteasome in plants. *Molecular Plant-Microbe Interactions* **27**, 611–623.
- Üstün S, Sheikh A, Gimenez-Ibanez S, Jones A, Ntoukakis V, Börnke F.** 2016. The proteasome acts as a hub for plant immunity and is targeted by *Pseudomonas* type III effectors. *Plant Physiology* **172**, 1941–1958.
- Villajuana-Bonequi M, Matei A, Ernst C, Hallab A, Usadel B, Doehlemann G.** 2019. Cell type specific transcriptional reprogramming of maize leaves during *Ustilago maydis* induced tumor formation. *Scientific Reports* **9**, 10227.
- Woloschuk RM, Reed PMM, McDonald S, Uppalapati M, Woolley GA.** 2020. Yeast two-hybrid screening of photoswitchable protein–protein interaction libraries. *Journal of Molecular Biology* **432**, 3113–3126.
- Zhang YL, Song GY, Lai NK, et al.** 2019. TurboID-based proximity labeling reveals that UBR7 is a regulator of N NLR immune receptor-mediated immunity. *Nature Communications* **10**, 1–17.
- Zhou BJ, Mural RV, Chen XY, Oates ME, Connor RA, Martin GB, Gough JL, Zeng LR.** 2017. A subset of ubiquitin-conjugating enzymes is essential for plant immunity. *Plant Physiology* **173**, 1371–1390.
- Zhou Z, Bi G, Zhou JM.** 2018. Luciferase complementation assay for protein–protein interactions in plants. *Current Protocols in Plant Biology* **3**, 42–50.